ANNUAL REVIEWS

*Annual Review of Physical Chemistry*

# Quantitative Mass Spectrometry Imaging of Biological Systems

Daisy Unsihuay, Daniela Mesa Sanchez, and Julia Laskin

Department of Chemistry, Purdue University, West Lafayette, Indiana 47907, USA; email: dunsihua@purdue.edu, dmesasan@purdue.edu, jlaskin@purdue.edu



Annu. Rev. Phys. Chem. 2021. 72:307–29

First published as a Review in Advance on January 13, 2021

The *Annual Review of Physical Chemistry* is online at physchem.annualreviews.org

https://doi.org/10.1146/annurev-physchem-061020-053416



## Keywords

quantitative mass spectrometry imaging, matrix effects, protein imaging, lipids, drugs, metabolites

## Abstract

Mass spectrometry imaging (MSI) is a powerful, label-free technique that provides detailed maps of hundreds of molecules in complex samples with high sensitivity and subcellular spatial resolution. Accurate quantification in MSI relies on a detailed understanding of matrix effects associated with the ionization process along with evaluation of the extraction efficiency and mass-dependent ion losses occurring in the analysis step. We present a critical summary of approaches developed for quantitative MSI of metabolites, lipids, and proteins in biological tissues and discuss their current and future applications.

## 1. INTRODUCTION

Mass spectrometry (MS) is a powerful analytical technique that enables the sensitive detection and identification of molecules in complex mixtures. With the advent of soft ionization techniques such as electrospray ionization (ESI) (1) and matrix-assisted laser desorption/ionization (MALDI) (2), MS became an indispensable tool for the label-free detection of intact biomolecules in biological samples. Dramatic improvements in the sensitivity, quantification, and identification capabilities of MS instrumentation have uniquely positioned it at the forefront of biological research, clinical studies, drug discovery, forensics, and environmental sciences. Meanwhile, the development of approaches for the spatial localization of molecules using MS imaging (MSI) has extended these strengths of analytical MS to the cellular and subcellular scales and enabled detailed molecular mapping of hundreds of molecules in biological tissues (3–9).

Absolute quantification is one of the key challenges in the MS analysis of complex mixtures (10, 11). Aside from instrumental parameters and sample preparation protocols, quantitative MS must address the complexity associated with dramatic variations in the ionization efficiency of different classes of compounds; signal suppression during the ionization of complex mixtures, also referred to as matrix effects; and the lack of appropriate standards (11). Relative quantification relies on an internal standard or a selected endogenous molecule in the sample to obtain the relative change in concentrations of other molecules in different samples. This approach is commonly used in untargeted profiling of the variations in the chemotype of a system at different conditions. Meanwhile, absolute quantification provides the absolute values of concentrations of analytes in the sample, making it much more challenging, particularly in the context of the complex mixture analysis that is of interest to this review.

A majority of quantitative MS studies of small molecules involve separation such as liquid or gas chromatography, which reduces the complexity of the analyte mixture. These studies typically rely on targeted techniques in which isotopically labeled standards are used to convert peak abundances observed in mass spectra into concentrations. In quantitative metabolomics (12, 13), the scarcity of standards may be addressed by employing microbial metabolism to generate libraries of isotopically labeled biomolecules. However, this approach still requires a substantial investment in the calibration and validation of the newly designed libraries of standards. In lipidomics (14), quantification typically uses two standards per lipid class that are selected from lipid species expected to be absent in the specific system under investigation. Correction factors are established to account for the differences in the ionization efficiency of lipids with different lengths and degrees of unsaturation of the fatty acyl chains (15). Several experimental approaches have been developed for absolute quantification in proteomics experiments. These techniques are not discussed here, and readers are referred to several excellent reviews on this topic (16, 17).

Since the initial demonstration of MSI by the Caprioli group (18), MALDI has become the most widely used soft ionization technique in MSI experiments, with several commercial platforms available to the scientific community (8, 9, 19, 20). The recent development of ambient ionization techniques, in which samples are analyzed without special pretreatment, has expanded the range of MSI applications (21–23). These ionization techniques can be classified into laser-based and liquid-extraction-based approaches (24). Laser ablation (LA) and LA coupled with ESI (LAESI) (25), along with matrix-assisted laser desorption ESI (MALDESI) (26), are among the most widely used laser-based ionization techniques in MSI. Meanwhile, most MSI experiments involving liquid-extraction-based techniques have relied on desorption ESI (DESI) (27, 28) and its variants along with nanospray DESI (nanoDESI) (29), liquid microjunction surface sampling probe (LMJ-SSP) (30), and liquid-extraction surface analysis (LESA) (31).

**Matrix-assisted laser desorption/ionization (MALDI):** an ionization technique in which a light-absorbing matrix is deposited onto a sample to assist the desorption and ionization of molecules with minimal fragmentation from interaction with a laser

**Mass spectrometry imaging (MSI):** an analytical technique that enables direct label-free spatial analysis of hundreds of molecules in biological samples by measuring their abundances at different locations in the sample

**Absolute quantification:** determination of the exact amount or concentration of an analyte of interest in a sample

**Matrix effects:** signal suppression or enhancement during ionization of complex mixtures due to competition for charge or differences in the efficiency of charged adduct formation

**Relative quantification:** determination of the relative change in an analyte concentration within or between the samples

Regardless of the ionization technique employed, MSI experiments always involve the simultaneous analysis of hundreds of molecules extracted from each location in the sample without chromatographic separation or sample cleanup. Furthermore, the addition of standards in MSI experiments is not straightforward. As a result, many quantification strategies developed for bulk sample analysis using MS cannot be directly applied to MSI. Despite these challenges, several approaches have been developed to facilitate quantitative MSI (QMSI). In this review, we focus on the most recent developments in QMSI, as earlier studies in this field have been previously reviewed (32–35). We present approaches for QMSI of metabolites, lipids, and proteins in biological tissues and discuss their current and future applications.

**Internal standard:** a molecule added to the sample for quantification experiments that accurately represents signal variations during ionization and transfer of analytes to a mass spectrometer

**Laser ablation (LA):** a technique in which molecules are ablated from a sample with the use of a laser

**Desorption electrospray ionization (DESI):** an ambient ionization technique in which molecules are removed from a sample by a stream of charged solvent droplets and ionized with minimal fragmentation

**Nanospray desorption electrospray ionization (nanoDESI):** an ambient ionization technique in which molecules are extracted from a sample into a dynamic liquid bridge formed between two capillaries positioned at an angle and ionized by ESI

## 2. MATRIX EFFECTS IN MASS SPECTROMETRY IMAGING

Matrix effects are common in MSI experiments (36, 37); however, the extent of signal suppression varies with the composition of the analyzed mixture. In tissue imaging, changes in the chemical composition of species extracted from different anatomical regions of heterogeneous tissue sections are the key factor determining the severity of matrix effects. Two types of matrix effects have been observed in MSI experiments: (*a*) ionization suppression due to the competition of molecules for charge and (*b*) signal enhancement or suppression due to variations in the alkali metal concentrations in different regions of the tissue sample (36, 38, 39). Regardless of their origin, matrix effects may affect the observed spatial localization of molecules and thereby the quantification of their concentrations in different parts of the tissue sample. As a result, compensation for matrix effects is necessary for accurate quantification in QMSI experiments.

### 2.1. Normalization Strategies

Different normalization strategies have been developed to compensate for matrix effects. The normalization of ion signals to the total ion current (TIC) is the most widely used approach in MSI experiments. Signal variations due to matrix effects are retained in ion images with TIC normalization. For example, Lanekoff et al. (36) used a middle cerebral artery occlusion (MCAO) stroke model in mice to illustrate the different types of matrix effects observed in the MSI of complex biological samples. In this experiment, the researchers performed nanoDESI MSI using a solvent containing two phosphatidylcholine (PC) standards, PC 25:0 and PC 43:6, supplied at a constant rate throughout the experiment. An optical image of the MCAO brain tissue section and ion images of both endogenous PC species and PC 43:6 standard normalized to the TIC and to the signal of an appropriate adduct of PC 25:0 are shown in **Figure 1**. The distribution of the signals of the sodium and potassium adducts of the standard shown in **Figure 1** is clearly not uniform, indicating the presence of matrix effects. First, the suppression of potassium adducts and the enhanced signals of sodium adducts of the same analyte molecules are observed in the ischemic region of the brain. This is attributed to differences in alkali metal concentrations caused by ischemia. Second, the high content of glycolipids in the white matter and the low ionization efficiency of these molecules result in an enhanced signal intensity of the PC standards in this region of the brain. These results demonstrate that normalization to the TIC cannot be used to compensate for these types of matrix effects.

Normalization to the standard has been used to generate ion images free of matrix effects, as shown in **Figure 1**. In this approach, the signals of endogenous PCs are normalized to the corresponding adduct of the PC standard. Normalization to the standard signal is a promising strategy for obtaining accurate concentration gradients of tissue sections using MSI. Multiple standards may be used to assess matrix effects for the different classes of lipids and metabolites observed in MSI experiments.

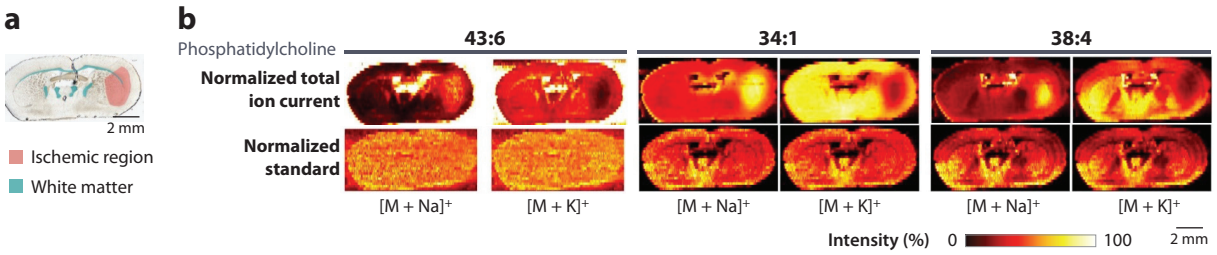


**Figure 1**

(*a*) An optical image of a middle cerebral artery occlusion brain tissue section with the ischemic region marked in pink and white matter marked in cyan. (*b*) Ion images of $[M + Na]^+$ and $[M + K]^+$ of the phosphatidylcholine (PC) 43:6 standard and endogenous PC 34:1 and PC 38:4. Ion images normalized to (*top*) the total ion current and (*bottom*) PC 25:0 standard are shown; the intensity scale bar ranges from 0% (*black*) to 100% (*light yellow*) signal intensity of an individual peak. Figure adapted from Reference 36; copyright 2014 The Royal Society of Chemistry.

**Liquid microjunction surface sampling probe (LMJ-SSP):** sampling probe composed of coaxial capillaries; solvent is delivered through the outer capillary and aspirated through the inner capillary, forming a liquid microjunction with the sample for direct analyte extraction

**Liquid-extraction surface analysis (LESA):** an ambient ionization technique in which molecules extracted from a sample into a static solvent droplet are subsequently transferred to a mass spectrometer inlet and ionized by nanospray ionization

**Total ion current (TIC) normalization:** a normalization method in which each peak abundance in the mass spectrum is divided by the sum of abundances of all the peaks

Several studies have used normalization over a region of interest instead of pixel-by-pixel normalization to compensate for regional matrix effects. In this approach, a tissue extinction coefficient (TEC) is used as a normalization factor to obtain normalized abundances of endogenous molecules extracted from the tissue. TEC is generally used to evaluate the analyte ion suppression either across different regions within the tissue or across different types of tissue. In one study, region-specific matrix effects were examined for a drug, olanzapine, that was evenly deposited onto mouse brain tissue (40). The authors used the graph-cuts algorithm to automatically cluster pixels from areas corresponding to different anatomical regions of the brain and calculated the region-specific TEC values shown in **Figure 2*a***. Direct comparison of the results obtained in DESI and MALDI experiments showed a fourfold decrease in TEC values in MALDI in comparison with those in DESI, indicating that olanzapine experienced higher ion suppression in MALDI experiments. Normalization of olanzapine signals to region-specific TEC values, shown in **Figure 2*b***, largely eliminates regional ionization suppression effects and enables the alignment of normalized intensities across clusters corresponding to different anatomical regions. Ion images of olanzapine are shown in **Figure 2*c***. With TIC normalization, olanzapine shows higher signals in white matter, indicating the presence of matrix effects. However, ion images normalized to TEC show a more uniform distribution of olanzapine across the tissue, which is consistent with the expected distribution of the deposited drug. The performance of this approach is highly dependent on the number of clusters used for the normalization; the characteristic anatomical features are still visible with 15 clusters (**Figure 2*c***) and are less prominent with 50 clusters (not shown).

## 2.2. Experimental Approaches

Other strategies that help to reduce matrix effects in MSI typically rely on sample preparation to obtain better control of the ionization process. Spraggins and coworkers (41) examined the effects of the matrix application approach and the properties of the matrix on the sensitivity of MALDI MSI toward different lipids using mouse liver tissue. Matrix selection affects the observed molecular profiles, types of adducts, and lipid coverage obtained using MALDI. For example, protonated species are more abundant when 1,5-diaminonaohtalene (DAN) and 9-aminoacridine (9AA) are used as matrices. Meanwhile, 2,5-dihydroxybenzoic acid (DHB), 5-chloro-2-mercaptobenzothiazole (CMBT), and 2,5-dihydroxyacetophenone (DHA) facilitate the formation of alkali metal adducts of analytes, with potassium adducts preferably formed when

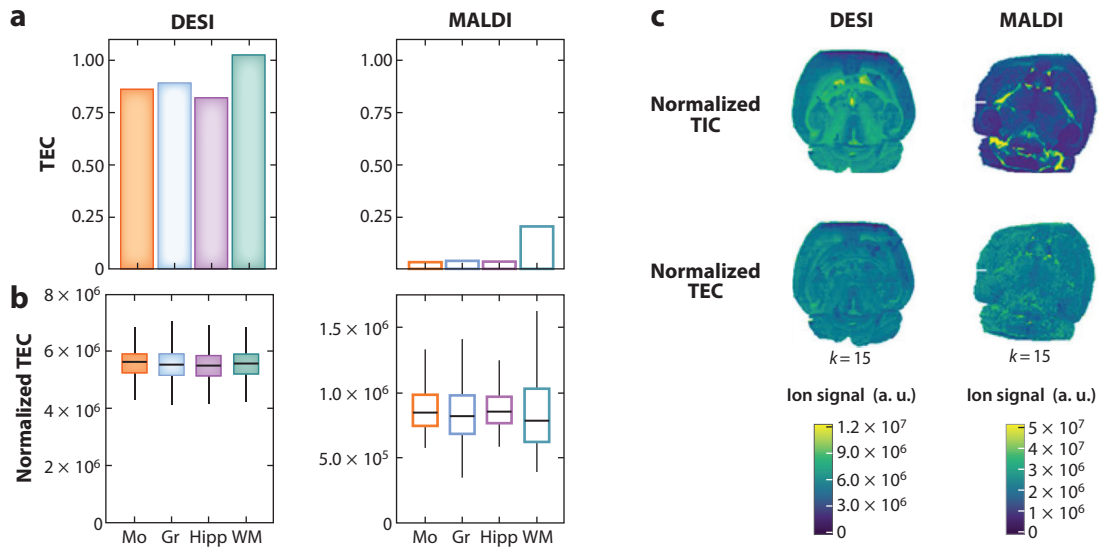


**Figure 2**

(*a*) Tissue extinction coefficient (TEC) and (*b*) normalized TEC values calculated in (*left*) desorption electrospray ionization (DESI) and (*right*) matrix-assisted laser desorption/ionization (MALDI) for olanzapine as an $[M + H]^+$ adduct (*m/z* 313.14) deposited on 10-μm mouse brain sections. Anatomical regions corresponding to the molecular (Mo) and granular (Gr) layers of the cerebellum, hippocampus (Hipp), and white matter (WM), which were successfully segmented using graph-cuts clustering, are indicated with different-colored bars. (*c*, *top*) Normalized total ion current (TIC) images of protonated olanzapine obtained with DESI and MALDI are shown, and (*bottom*) normalized ion images of protonated olanzapine by cluster-specific TECs are shown for 15 clusters. Figure adapted with permission from Reference 40; copyright 2018 American Chemical Society.

DHA is used as a matrix. The matrix application method mainly affects the types of adducts generated in the ionization process. Alkali metal adducts are preferentially formed when the matrix is applied using spray coating, whereas matrix sublimation onto the tissue favors the formation of protonated molecules. This study demonstrated that better understanding of the physicochemical processes occurring at the tissue–matrix interface is important for controlling the molecular profiles observed in MALDI MSI. We note that matrix effects should not be confused with the effect of the matrix in MALDI experiments. However, understanding the effect of the matrix provides important insights into the origin and extent of matrix effects in MALDI MSI.

Different matrices have been examined to enhance the sensitivity of low-abundance analytes for accurate quantification. For example, Yang et al. (42) found that an α-cyano-4-hydroxycinnamic acid (CHCA) matrix was best suited for the detection of the environmental organic pollutant perfluorooctanesulfonic acid (PFOS) in mouse kidney. PFOS was preferentially detected in negative mode, likely due to its acidity ($pK_a < 1$), and with the highest intensity in the CHCA matrix among all other surveyed matrices. Likewise, Rzagalinski et al. (43) used a 2-[(2*E*)-3-(4-tert-butylphenyl)-2-methylprop-2-enylidene] malononitrile (DCTB) matrix to improve the sensitivity of MALDI to five central nervous system drugs: xylazine, imipramine, clozapine, ketamine, and clonidine. Although standards of all five drugs by themselves exhibited the highest signal intensities when CHCA was used as a matrix, DCTB was the preferred matrix for the analysis of the standards mixed with brain tissue homogenate. The increased signal suppression by CHCA was evaluated by calculating the TEC values, which showed an eightfold increase in suppression factor with the CHCA matrix than with the DCTB matrix. For the quantification of xylazine in mouse brain, this difference represented a nearly 100-fold increase in signal intensity in single pixels and an

**Tissue extinction coefficient (TEC):** ratio of the mean signal intensity of the analyte in a selected region of the tissue to its signal obtained off the tissue (e.g., on a glass slide)

upward of 400-fold increase in ion abundances observed using DCTB in comparison with using the CHCA matrix. Despite DCTB being traditionally considered an electron-transfer matrix, the calculated gas-phase proton affinity of DCTB (866 kJ/mol) is similar to that of CHCA (863 kJ/mol) and significantly lower than those of the studied drugs xylazine (1,018 kJ/mol) and ketamine (964 kJ/mol). Therefore, proton transfer from protonated matrix molecules to the desorbed analytes may be responsible for the efficient detection of this series of drugs using DCTB.

Ionization suppression of small metabolites can be reduced using matrix additives. Ammonium sulfate (AS) has been used as a matrix additive to improve the signal from hydrophilic quaternary ammonium compounds such as carnitine, acetylcarnitine, and phosphocholine (44). These compounds are generally suppressed in MALDI experiments due to the presence of more readily ionizable molecules. A properly selected matrix additive helps to increase the signal of these compounds by suppressing the signals of more abundant species, including PCs and clusters derived from the DHB matrix. In the presence of 63-mM AS in the matrix, MALDI favors the formation of protonated species and suppresses the formation of alkali adducts. Such high concentrations of AS are believed to cause the so-called salting out of several classes of molecules, reducing their solubility. In contrast, quaternary ammonium compounds are efficiently extracted and cocrystalized with the DHB matrix in the presence of AS. Although the molecular coverage obtained using this approach is substantially reduced, five quaternary ammonium compounds that have not been observed using other matrices could be spatially localized by adding AS to the matrix.

On-tissue derivatization strategies have been explored for the QMSI of low ionization efficiency compounds using MALDI. For example, Barré et al. (45) used Girard's reagent T (GT) to derivatize triamcinolone acetonide (TAA), an osteoarthritis drug, which is otherwise nearly undetectable with ESI or MALDI. In this study, the tissue coated with GT was incubated for 2.5 h at 40°C prior to analysis. This strategy was used to quantify and visualize the spatial distribution of TAA. Derivatization resulted in a 78-fold increase in the TAA signal and allowed the quantification of TAA penetration into cartilage. A homogenous distribution of TAA in the cartilage was observed after a 48-h incubation with the drug.

Similarly, ambient liquid-extraction-based techniques have exploited different strategies to improve both the extraction and ionization efficiencies of targeted molecules. Solvent composition may be optimized to improve analyte extraction based on its polarity. For example, methanol/water mixtures are commonly used for the extraction of polar molecules, whereas solvents containing nonpolar components are used to improve the solubility of less polar molecules (46). In DESI experiments, dimethylformamide has been used to preserve the morphological structure of tissue sections (47). The ionization efficiency of poorly ionizable molecules may be improved using ionization enhancers that facilitate the cationization of analytes generally detected in negative mode. This approach has been used for the imaging of prostaglandins using complexation with $Ag^+$ (48) and phosphoethanolamines by forming a complex with a synthetic dication (DC9) (49). Online derivatization also has been used to improve the sensitivity of ambient ionization techniques toward neutral molecules. For example, betaine aldehyde selectively reacts with alcohol groups, which enables the imaging of neutral sterols (50).

## 3. QUANTITATIVE MASS SPECTROMETRY IMAGING OF SMALL BIOMOLECULES IN TISSUES

Differences in sample preparation for imaging experiments necessitate different QMSI approaches for the imaging of small biomolecules (e.g., lipids, metabolites, and drugs) in tissue sections. In the following section, we discuss these approaches for several classes of ionization techniques.

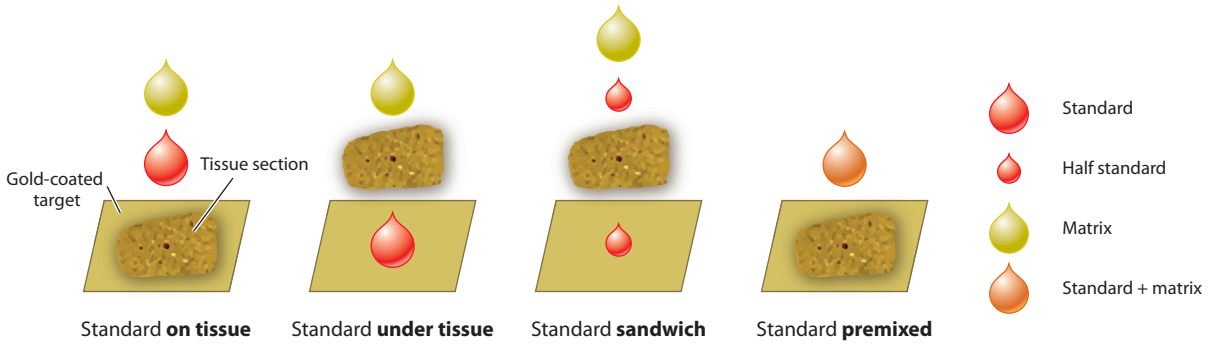


**Figure 3**

Illustrations of the four methods of applying standards for mass spectrometry imaging. Depositing the standards on the tissue section requires thaw-mounting the section followed by application of the standards and matrix. Deposition under the tissue section requires spotting the standards first, thaw-mounting the section on top of them, and then applying the matrix. A sandwich method combines depositing the standards under and on the tissue section followed by application of the matrix. Premixing the standard involves thaw-mounting the tissue section followed by depositing the standards and the matrix in a single solution. Figure reproduced with permission from Reference 52; copyright 2016 American Chemical Society.

## 3.1. Matrix-Assisted Laser Desorption/Ionization and Related Techniques

Quantitative strategies for MALDI and other related laser-based techniques are dominated by two main approaches: on-tissue spotting of standards and mimetic models (51). A third so-called in-solution approach, in which standards are applied to an off-tissue region and correlated using the TEC factors, exists but has largely fallen out of fashion in recent years as it is thought to be less reliable. In each approach, several concentrations of a standard (often an isotopically labeled analog of the target analyte) are used to generate a standard curve that can then be utilized to correlate ion signals observed in imaging experiments to known concentration values. However, both the on-tissue spotting and the mimetic model approaches require significant sample preparation, which we discuss here.

**3.1.1. On-tissue spotting of standards.** On-tissue spotting is performed using one of the four methods illustrated in **Figure 3**:

1. spotting of the standard directly on top of the tissue followed by matrix application,
2. spotting of the standard directly on the glass slide followed by mounting of the tissue and subsequent matrix application,
3. spotting using a sandwich method in which half of the standard is applied directly on the glass followed by tissue mounting and spotting of the other half of the standard on top of this tissue prior to matrix application, and
4. incorporation of the standard into the matrix itself.

Chumbley et al. (52) compared these methods using the drug rifampicin in liver tissue. Although quantification values for all of the techniques were comparable, the first method, in which the standard is spotted directly on top of the tissue, produces quantitative values most consistent with high-performance liquid chromatography (HPLC)-tandem mass spectrometry (MS/MS) results from a dosed-tissue homogenate. Meanwhile, premixing the standard with the matrix produced somewhat lower concentrations. Although the origin of this effect has not been thoroughly investigated, the partitioning of the analyte into the crystals may be affected by the presence of a similar molecule already uniformly premixed with the matrix. Alternatively, cocrystallization of

the standard and matrix on the tissue may enhance its ionization efficiency. Subsequently, the standard is preferentially ionized, whereas the analyte is only partially extracted. This results in lower calculated concentrations of the analyte upon normalization. Conversely, application of the standard under the tissue or partly under the tissue in the sandwich method results in concentrations higher than the ones obtained using HPLC-MS/MS and, furthermore, introduces greater experimental variability. This is attributed to the inconsistent or poor penetration of the standard through the tissue for subsequent extraction into the matrix crystals, which thereby leads to a lower than expected abundance of the standard.

**Mimetic tissue model:** a simplified model of a real tissue prepared from a tissue homogenate spiked with known concentrations of internal standards; the model helps to account for matrix effects and enables quantification

**3.1.2. Mimetic tissue model.** Similar to the on-tissue QMSI strategy, the mimetic tissue model approach requires prior sample preparation. Several mimetic tissue preparation protocols have been developed to ensure accurate quantification in QMSI experiments. Generally, these protocols use homogenate mixtures of the target tissue spiked with one or more standards at different concentrations. This approach requires the assumption that the signal of the standard observed in the analysis of such tissue homogenate adequately represents the matrix effects experienced by the appropriate analytes examined in QMSI experiments (53). Although tissue homogenate cannot be used to evaluate differences in matrix effects in different anatomical regions of the analyzed tissue, it facilitates accurate quantification for systems in which such effects are not particularly pronounced.

A mimetic tissue preparation protocol shown in **Figure 4** uses serially frozen spiked-tissue homogenate layers in a cylinder to create a single cross section with a concentration gradient that can be mounted with the experimental tissue for easier analysis (54). Special care is taken to

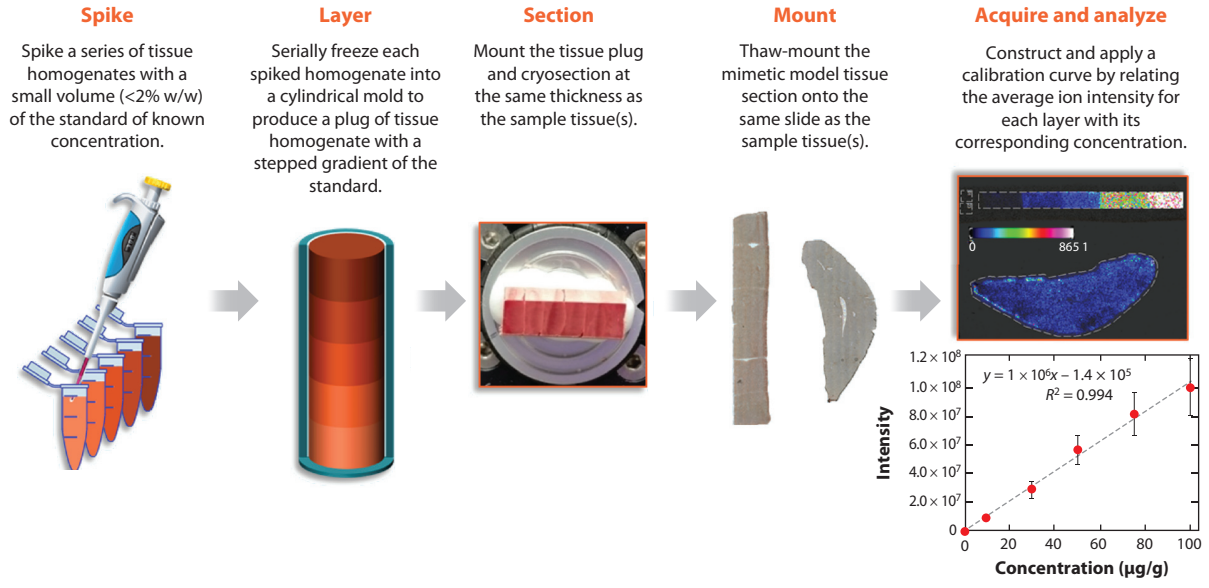


**Figure 4**

Schematic illustrations outlining the workflow for the generation and application of a mimetic tissue model for quantitative mass spectrometry imaging. The process involves spiking tissue homogenates with low volumes of standard and serially freezing these solutions into a mold. The resulting tissue plug is then sectioned alongside the target tissue and mounted to the same sample target. Weighted linear regression can then be applied to correlate the average ion intensity of each layer of the model to its corresponding final tissue concentration. Figure adapted from Reference 54 (CC BY 4.0).

minimize the spiked standard solution volume (in this case, clozapine below 3% w/w) to maintain native tissue density. Mimetic models for liver, kidney, and brain tissue have been prepared, but only liver and brain models were validated using liquid chromatography (LC)-MS, resulting in 1.5% and 2.1% errors, respectively. Another recent methodology for mimetic model construction incorporates native cells and a hydrogel scaffold component in addition to tissue homogenate to generate a 3D biomimetic tissue (55). To do this, tissue is homogenized in the presence of a 2.5% agarose saline solution, spiked with the appropriate standard, combined with a concentrated organ-derived cell suspension, and left to set for 10–15 min. The reincorporation of native cells that do not survive the homogenization process may better replicate the native tissue structural integrity. The relative deviation between ionization efficiencies of a spiked drug for this model tissue and the real tissue was less than 15%, though no comparison was made to other spiked-homogenate protocols.

**3.1.3. Examples of quantitative mass spectrometry imaging applications.** Both the on-tissue spotting and mimetic model strategies have been used in many applications, some of which are described here. Giordano et al. (56) used an on-tissue approach to better understand the roles of structural heterogeneity and tumor microenvironment by quantifying the drug penetration of paclitaxel in a malignant pleural mesothelioma tumor model via a 3D imaging experiment. This imaging experiment analyzed multiple sequential sections from the same tumor, which were then computationally reconstructed into a 3D model to visualize the paclitaxel penetration. Predictably for malignant pleural mesothelioma, a highly heterogeneous neoplasm with high resistance to drugs, paclitaxel was primarily concentrated on the tumor edges in only about 0.21% of the tumor volume. The remaining paclitaxel was found at low concentrations ($<0.2$ μg/g, below the limit of detection) in 37.7% of the tissue volume. Notably, this experiment showed paclitaxel in higher concentrations in and around non-necrotic areas and in low concentrations around fibrotic and necrotic regions of the tumor. This finding corroborates the hypothesis that hypoxic tumor areas are especially difficult for chemotherapeutics to reach and thus may be the sites of tumor resistance and reemergence.

Nazari et al. (57) used the on-tissue approach to quantify an endogenous metabolite, glutathione (GSH), in hen ovarian tissue using a related laser-based technique, infrared (IR)-MALDESI. In this experiment, age-matched healthy and cancerous tissues were compared, and a dilution series of stable isotope–labeled GSH pipetted on top of tissue was used to generate a calibration curve. An acute increase in GSH concentration was observed in cancerous tissue, and a heterogeneous distribution was seen in both tissue types. Although the absolute GSH concentrations calculated from the IR-MALDESI experiment were twice as high as those with LC-MS/MS, the approximately twofold change between healthy and cancerous tissue was consistent between both techniques.

In addition, GSH in human ocular lens was quantified using a mimetic model to better understand the aging-related development of lens cataract formation (58). Tissues from four donors, ranging in age from 29 to 82, were analyzed. GSH was found to decrease with increasing age, primarily in the nuclei of the cells. However, some biological variability was noted, with the lowest GSH concentrations present in the sample from the second-oldest donor (74 years of age; 2.7 μmol/g tissue in the cortex and 0.8 μmol/g in the nucleus). These values agree with the average literature values generated using alternative quantitative techniques. To further validate the use of a homogenous mimetic model for the quantification of GSH in different regions of the lens, ion suppression between cortex and nucleus was tested and found to be minimal (approximately 3%). This study also examined other small metabolites including ceramides, which localized in areas of the lowest GSH concentration and showed a signal increase with a decrease in nuclear GSH.

The repeatability and reproducibility of QMSI based on mimetic models were examined for the quantification of the drug clozapine and its major metabolite norclozapine in perfused rat liver (59). Despite some differences in the sampling regions used for QMSI and LC-MS/MS analyses, this study found 84% and 82% accuracy in the quantification of clozapine and norclozapine, respectively, in comparison to LC-MS/MS. Accuracy was determined from the mean of pooled MSI data acquired by three different analysts with six replicates (serial tissue sections) each at three separate locations, while LC-MS/MS analysis was done at the same site. The repeatability of the technique was determined by the intra-analyst precision [percent relative standard deviation (RSD)] and was found to be 12% for both clozapine and norclozapine upon normalization to an isotopically labeled standard, clozapine-d8. However, nonnormalized values were 8% and 7% for clozapine and norclozapine, respectively, which more closely matched the 8% RSD from LC-MS/MS analysis. Reproducibility was described by pooling of all the replicates examined by the three analysts. For clozapine, reproducibility was 13% and 14% for normalized and nonnormalized values, respectively. However, reproducibility for norclozapine significantly worsened to 27% when normalized to the standard compared to the raw value of 13%. The slight worsening in accuracy and substantial worsening in reproducibility upon normalization could be attributed to differences in the extraction efficiency of analytes from the heterogeneous tissue matrix in comparison to the homogeneously surface-coated standard. This results in an exaggerated correction by normalization and thereby largely mismatched variances, a phenomenon that has been previously investigated. Therefore, normalization to a standard is generally best used when the ratio of the analyte and standard signal is close to unity. In general, the low RSD values reported in this study are an encouraging result toward the validation of MALDI QMSI.

**3.1.4. New experimental approaches.** Several studies have highlighted important experimental considerations in MALDI QMSI beyond the sample preparation strategies. For example, Porta et al. (34) optimized laser energy and sample stage velocity to avoid analyte carryover and minimize intraspot variability, respectively. Moreover, the authors examined the effects of the frequency and number of laser shots per pixel on the intraspot variability and, therefore, the accuracy of quantification. This study demonstrated that an average of four to five pixels is best suited for accurate quantification, such that instrumental variability and matrix heterogeneity are confidently accounted for.

Abundant matrix peaks in the low mass-to-charge ratio (*m/z*) range present a challenge for the MALDI QMSI of small biomolecules, which is typically addressed using MS/MS. A high-speed tandem time-of-flight (TOF/TOF) system has been used to acquire multiple TOF/TOF events in a single laser shot (60, 61). This technique enables the acquisition of MS/MS spectra of both the analyte and standard in the same laser shot, which enables the normalization of the analyte signal to the standard signal in each pixel and thereby reduces signal variability in QMSI. As illustrated in **Figure 5**, an ion gate is pulsed multiple times (**Figure 5*b*,*d***) to isolate multiple precursor ions generated in the same laser shot. Following fragmentation, the ions are reaccelerated (**Figure 5*d*,*f***) into the TOF-2 region of the instrument. The resulting spectrum contains both fragments and precursors for both the analyte and standard (**Figure 5*g***), allowing for the normalization of signals from the same laser shot. Quantification is performed by on-tissue spotting of a dilution series of the standard to generate a calibration curve. This multiplexed approach has been validated by quantifying rifampicin (*m/z* 821) with a rifapentine standard (*m/z* 876) in human plasma and a rabbit liver model. The RSD of rifampicin was 5.1% in a spotted human plasma experiment, a fourfold improvement in comparison with conventional MALDI MS/MS. A more conservative decrease, from 24.9% RSD without normalization to 15.2% with normalization to the standard, was observed in a rabbit liver QMSI experiment. The accuracy was also improved, with an

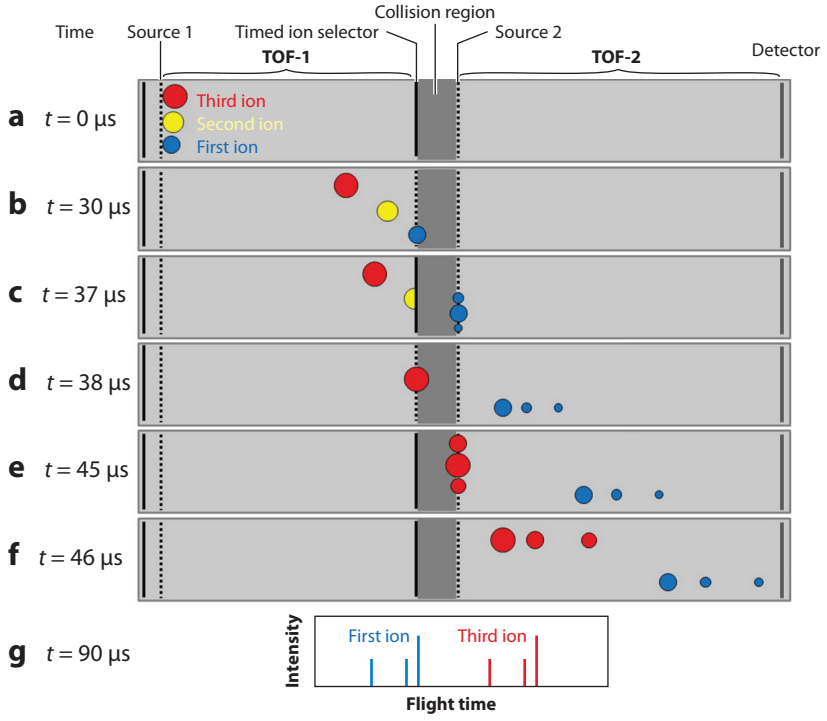


**Figure 5**

Schematic illustration of a high-speed tandem time-of-flight (TOF/TOF) system for the acquisition of multiple TOF/TOF events in a single laser shot. (*a*) Ions enter the instrument and are separated by mass-to-charge ratio in TOF-1. (*b*) The ion gate is opened to allow the passage of the first ion (*blue*) into the collision cell. (*c*) The ion gate closes to prevent the second ion (*yellow*) from entering into the collision cell, while the first ion and its fragments enter the reacceleration zone. (*d*) The ion gate opens once again to allow the third ion (*red*) passage into the collision cell as the first ion and its fragments are reaccelerated into TOF-2. (*e*) The third ion and its fragments enter the reacceleration zone while the first ion and its fragments are separated by mass-to-charge ratio in TOF-2. (*f*) The third ion and its fragments are reaccelerated into the TOF-2 region. (*g*) Combined spectra of both the first and the third ions and their respective fragments are obtained. The combined tandem mass spectrometry (MS/MS) spectra from a single laser shot allows the normalization of the analyte signal to the standard signal with lower shot-to-shot variability. Figure adapted with permission from Reference 60; copyright 2016 American Chemical Society.

increased linear-squares correlation coefficient and an average error (calculated by $1/x^2$ weighted linear regression) decrease from 14.4% to 8.2% for spotted human plasma after normalization to the standard, and a marked decrease from 48.3% to 6.3% average relative error ($1/x^0$) in the MSI experiment. MSI quantification of the rabbit liver model agreed, with only a 10.6% difference from LC-MS/MS results.

**3.1.5. Advanced data processing.** Deepaisarn et al. (62) have also explored improved data analysis approaches to reduce signal variability in MSI. Poisson statistics more accurately describes the signal and noise variability in MALDI than the commonly assumed Gaussian statistics. The researchers compared quantification results obtained using ratios of individual peaks in MALDI spectra to the results obtained using linear Poisson independent component analysis. In this analysis, each component represents a correlated set of peaks with peak intensities described by

Poisson statistics. Using this approach, a twofold increase in RSD was found for multiple samples, including milk and extracts of lamb brain and liver tissues, in comparison with a traditional peak ratio analysis. However, single peak ratios may not be appropriate for quantification in MALDI experiments.

## 3.2. Ambient Liquid-Extraction-Based Techniques

In liquid-extraction-based techniques, including LMJ-SSP, nanoDESI, LESA, and single probe, molecules are extracted from a specific location on a tissue into a solvent and subsequently ionized by ESI or nanoESI.

**3.2.1. Online addition of standards.** For quantification, standards are added to the extraction solvent and are analyzed with the extracted analyte mixture. Relative quantification is performed by normalizing the signal of the extracted analyte of interest to the standard signal. Meanwhile, absolute quantification requires an additional step in which the extraction efficiency from different parts of the tissue is determined. A complete extraction may not be achieved on the timescale of the sampling process. For example, Lanekoff et al. (38) reported ~9% extraction efficiency of nicotine in nanoDESI MSI of dosed rat brain tissue, indicating that nicotine was extracted from the top 1-μm layer of the tissue section. Meanwhile, Kertesz et al. (63) demonstrated that the extraction efficiency of propanolol using LMJ-SSP in brain, kidney, and liver tissues of 10-μm thickness was in the range of 45–63%. The extraction efficiency likely depends on the type and thickness of the tissue section, the properties of the analyte and extraction solvent, and the scan rate and spatial resolution of the MSI experiment. If the extraction efficiency is known, absolute quantification is straightforward. This approach has been used both for targeted quantification of drugs and metabolites (38) using deuterated standards and for a shotgun-like quantification of lipids (64) using only one or two standards per lipid class. QMSI of small neurotransmitters in rat brain tissue using nanoDESI showed good reproducibility but fairly large standard deviations, which were attributed to both technical and biological variations between different tissue sections (39).

A modified approach has been developed for quantitative nanoDESI imaging of prostaglandins (PGs), important signaling molecules present at low concentrations in tissue samples that are difficult to ionize using traditional approaches (48). In this approach, acetonitrile containing 10 ppm of $Ag^+$ was used as the extraction solvent. $Ag^+$ ions interact with double bonds, thereby improving the ionization of unsaturated molecules such as PGs. Complexation with $Ag^+$ resulted in a 30-fold increase of PG signals. QMSI experiments with mouse uterine tissue sections were performed by adding a deuterated PG standard to the extraction solvent and normalizing the signals of endogenous PGs to the standard signals. Quantitative nanoDESI ion images revealed the preferred localization of PG species to both the luminal and glandular epithelia in the uterine tissue and provided for the first time the distribution of PG concentrations across the sample. $PGE_2$ was the most abundant species among the five PGs detected, reaching concentrations of ~320 nM in the luminal epithelium.

Absolute quantification using direct liquid-extraction-based techniques is mainly hindered by difficulties in quantifying the extraction efficiency across different regions of the tissue. An almost complete extraction may be achieved either by placing a probe onto a sample for an extended period of time (65) or by excising tissue punches (63, 66) for subsequent off-line solvent extraction. Such spatially resolved sampling of tissues is assisted by either LC-MS or LC-MS/MS analysis. Wu et al. (67) used this approach for the quantitative spatial profiling of sphingolipids in rat brain tissue by coupling LMJ-SSP to LC-MS. The extraction efficiency of ~80% was achieved

by adding 1,1,1,3,3,3-hexafluoro-2-propanol (HFIP) to methanol. An exhaustive surface sampling was carried out by placing the LMJ-SSP probe on the tissue for 2 min followed by 14 min of LC-MS analysis. Spot-by-spot quantification was achieved by adding the appropriate lipid standards to the extraction solvent. Quantitative ion images of sphingolipids in rat brain were validated using bulk-extraction LC-MS. The calculated concentrations of different cerebroside species were in the range of 3–45 $\mu g/mm^3$ in the fiber tracts region and 1–30 $\mu g/mm^3$ in the midbrain region. Despite the accuracy and molecular coverage obtained using this approach, improvements to the spatial resolution and throughput are still needed to make it more compatible with the demands of MSI experiments.

**3.2.2. Standards deposited on tissue or prepared with a tissue homogenate.** The mimetic tissue model has been used to quantify concentrations of drugs in LESA and DESI MSI (68). LESA was used to create an external calibration curve from liver mimetics spiked with varying concentrations of olanzapine, moxifloxacin, erlotinib, and terfenadine. Quantification of these drugs in dosed rat liver tissue sections using LESA MSI and DESI MSI produced comparable results. Specifically, concentrations of olanzapine, moxifloxacin, erlotinib, and terfenadine at 2 h post-dose with LESA MSI were 9.3, 15.6, 38.4, and 11.9 nmol/g, respectively, and 14.4, 10.8, 26.9, and 12.0 nmol/g, respectively, with DESI MSI.

Quantification of analytes deposited onto a sample has been used to examine the validity of QMSI experiments performed using spray-based techniques including DESI and its analogs. Homogenous deposition of the analyte is key to accurate quantification and may be achieved using micropipetting, spraying, and inkjet printing (69).

Chemical reagents also have been deposited onto the tissue for selective derivatization of targeted molecules. This on-tissue derivatization approach was used by Shariatgorji et al. (70) to improve the sensitivity of detection of neurotransmitters and neuroactive drugs containing primary amino groups via their reaction with pyrylium salts. Quantitative DESI MSI was performed for the drug fluvoxamine in brain tissue sections. In this experiment, deuterated fluvoxamine (fluvoxamine-d4) was deposited onto the tissue along with the pyrylium salt 2,4-diphenylpyranylium tetrafluoroborate (DPP-TFB) reagent. Due to the presence of the derivatizing agent, both the drug and the standard undergo conversion to their corresponding pyridinium cations. Aliquots of 0.2 $\mu L$ of fluvoxamine at concentrations ranging from 0.02 mg/mL to 0.032 $\mu g/mL$ using a dilution factor of five were spotted on control tissue sections as shown in **Figure 6*a***. A calibration curve was constructed by plotting the derivatized fluvoxamine/fluvoxamine-d4 ratio against the amount of fluvoxamine spotted onto the tissue section (**Figure 6*b***). Fluvoxamine-dosed tissue sections in **Figure 6*c*** show preferred localization in the ventral striatum, thalamic, and cerebellar regions of the brain. **Figure 6*d*** shows the quantification of dosed fluvoxamine in different parts of the brain using the average spectrum in every specific structure. The highest concentration of fluvoxamine of ~100 pmol/mg of tissue was found in the ventral striatum.

An interesting strategy recently reported in the literature (71) introduces the concept of virtual calibration to account for regional matrix effects without the use of synthetic standards. In this approach, region-specific endogenous metabolites strongly correlated to the ion intensity changes of the analyte are selected as the so-called native internal standards and are used to assess matrix effects. A machine-learning regression model is used to fit the relationship between the signal intensities of the standards and that of the analyte in different types of tissue. This training model is applied to predict a relative calibration factor ($f_r$) that is used to correct the signal of the analyte ($I_{pix}$) in every pixel. For quantification, an external calibration curve is constructed using a mimetic tissue that correlates the calibrated signal of the analyte ($I_{pix}/f_r$) to its concentration. Using this approach and liver mimetic sections for calibration, the concentration of a drug candidate coded

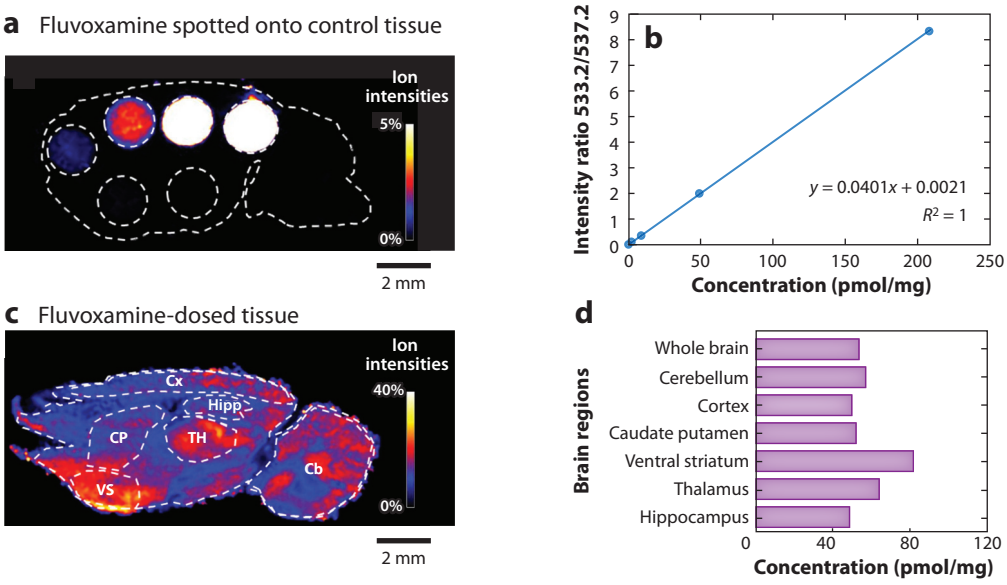


**Figure 6**

Quantification of fluvoxamine via on-tissue derivatization with DPP-TFB. (*a*) Different concentrations of fluvoxamine ranging from 0.02 mg/mL to 0.032 μg/mL using a dilution factor of five spotted onto control tissue sections previously sprayed with fluvoxamine-d4. The lateral scale bar represents 2 mm; the intensity scale bar range (0–5%) is indicated on the right side of the panel. (*b*) Graph showing the calibration curve using different intensity ratios of fluvoxamine/fluvoxamine-d4 at different concentrations of fluvoxamine from panel *a*. (*c*) DPP-TFB-derivatized fluvoxamine in dosed tissue. The intensity scale bar range (0–40%) is again indicated on the right. (*d*) Graph showing the quantification of fluvoxamine in different regions of the brain. Abbreviations: Cb, cerebellum; Cx, cortex; CP, caudate putamen; DPP-TFB, 2,4-diphenyl-pyranylium tetrafluoroborate; Hipp, hippocampus; TH, thalamus; VS, ventral striatum. Figure adapted with permission from Reference 70; copyright 2016 Elsevier.

as LXY6006 was quantified over a whole body section. Ten endogenous metabolites were selected as standards. A comparison of the calibration factors obtained from different organs revealed that matrix effects are more dominant in heart and lung tissues. Matrix effects were effectively accounted for using virtual calibration, and the concentration of the drug was quantified in every organ. The researchers found that the drug preferentially accumulated in the heart, reaching a concentration of 3 pmol/mm$^2$, which agrees well with the concentration of 4 pmol/mm$^2$ calculated using the TEC approach. Although this study was carried out using a spray-based technique, it can be readily extended to laser- or plasma-based techniques.

## 4. PROTEIN IMAGING

### 4.1. Quantitative Imaging of Intact Proteins

Soft ionization techniques have traditionally been used for imaging intact proteins (72–74). Most of the studies in this field employed MALDI MSI and were focused on the spatial localization of the proteins rather than on quantification. The quantification of intact proteins observed in MSI experiments is challenging due to the uncertainty in the ionization efficiency and signal suppression in different parts of the tissue. Recently, the mimetic tissue model has been used for the quantification of ubiquitin in MSI experiments performed using LESA (75). Specifically, a homogenized rat brain tissue spiked with $^{13}$C, $^{15}$N–labeled ubiquitin was used as a mimetic model. The mimetic tissue model material was sectioned and analyzed alongside rat brain tissue sections.

A calibration plot obtained at different concentrations of the isotopically labeled ubiquitin in the mimetic tissue sample provided the upper limit of quantification of 163 nmol/g tissue. The average concentration of ubiquitin across the rat brain tissue was around 130 nmol/g, which is consistent with the LC/MS data. This study established an approach for the targeted quantification of proteins in tissue sections in LESA-MSI experiments that can be readily extended to other sampling and ionization techniques.

Protein identification is one of the biggest challenges in MSI experiments. One experimental strategy designed to address this challenge involves on-tissue enzymatic digestion followed by imaging of the resulting peptides (73). The development of nanoPOTS (nanodroplet processing in one pot for trace samples) (76), a highly sensitive platform that enables a complete proteomics workflow to be performed in an ~200 nL volume of solvent, has opened up unique opportunities for both the imaging and identification of thousands of proteins in tissue sections with a spatial resolution of better than 100 μm (77). In this experiment, tissue voxels are generated using laser capture microdissection and capture of the excised tissue into individual nanowells on a specially designed chip. An automated proteomics workflow performed in the nanowells includes protein extraction and denaturation, then alkylation, digestion, and transfer to a 96-well plate for subsequent analysis by LC-MS/MS. A log transformation of the relative peptide abundances followed by normalization and roll up from scaled peptide abundances to the protein level yields the normalized relative protein abundances. This approach enables relative quantification by comparison of the abundance of the same protein in different voxels. NanoPOTS was employed to obtain >2,000 protein images in mouse uterine tissues on day 4 of pregnancy. The results were validated against bulk analysis of the different cell types present in the tissue. This study provided a detailed proteomics map of the distinct cell types in the tissue. It also demonstrated how protein localization is linked to important biochemical processes in this system. For example, proteins related to the remodeling of the extracellular matrix in preparation for embryo implantation were found to be enhanced in stroma. Meanwhile, proteins related to epithelial cell crypt formation were found to be localized to the luminal epithelium.

**Inductively coupled plasma mass spectrometry (ICP-MS):** a technique in which a sample is atomized and ionized in plasma generated in argon by an oscillating high-frequency electromagnetic field

## 4.2. Quantitative Elemental Imaging of Metals and Proteins in Biological Samples

Inductively coupled plasma mass spectrometry (ICP-MS) is an established technique for the quantitative elemental analysis of complex samples (78). Under typical ICP conditions, analyte molecules are completely dissociated into their atomic constituents and small polyatomic ions, which are subsequently analyzed using mass spectrometry. Accurate quantification is possible because the ionization efficiency is compound independent and, therefore, ion abundances are directly correlated to the elemental composition and concentration of each compound (79). The coupling of LA with ICP-MS (LA-ICP-MS) (80, 81) enables the spatial elemental profiling of biological samples (82, 83). The technique offers lower than parts-per-million detection limits, up to nine orders of magnitude dynamic range, and down to 1-μm spatial resolution.

By combining LA-ICP-MS with immunohistochemical staining using lanthanide-labeled antibodies, Giesen et al. (84) have extended the capabilities of this technique to the targeted imaging of proteins in tissues. In this study, three tumor markers (MUC1, Her2, and CK7) were detected in formalin-fixed, paraffin-embedded tissues of human breast cancer. Although signal intensities in LA-ICP-MS experiments increased with tissue thickness, the authors reported that best-quality results were obtained using 5-μm-thick sections, which are less likely to crack during LA. Other important conditions included laser energy, spot size, and scan rate along with antibody concentration and incubation time.

**Elemental fractionation:** a differential loss of certain elemental and molecular components due to processes occurring in the ablation plume that alters the relative abundance of peaks in the mass spectrum

In both elemental and protein imaging by LA-ICP-MS, quantification typically relies on matrix-matched standards, which are not always available (79). In an ideal LA experiment, all the elements are removed from the sample and transported to the ICP-MS with the same efficiency. One of the key issues is elemental fractionation, which is affected by the physical properties and chemical composition of the sample along with laser wavelength, pulse duration, energy, and repetition rate. Fractionation is less pronounced in experiments using femtosecond lasers, which generate high-quality craters and more monodispersed particles in the ablation process.

The experimental factors affecting quantification in LA-ICP-MS include fluctuations in laser power output, variations in transport efficiency and amount of ablated material, and signal instability. The selection of appropriate standards for LA-ICP-MS experiments is challenging and is usually limited to elements present in the sample matrix; standard should be present in the sample at a known concentration. For tissue samples, $^{13}C$ is typically used for quantification. Typical percent RSD obtained in these experiments is below 10%. However, the assumption that carbon concentration is constant across a tissue section is difficult to justify, and there is experimental evidence that variations in the chemical composition of carbon-rich matrices may affect the accuracy of both $^{12}C$- and $^{13}C$-based normalization strategies. Furthermore, differences in the partitioning of carbon and other elements within the particle phase and into the vapor phase in the ablation plume demonstrated for polymer samples must be quantified for biological samples to verify the robustness of carbon isotopes as standards (85).

Other normalization approaches rely on the measurement of the ablated mass using acoustic or optical techniques. It is assumed both that similar particle distributions are generated in the ablation of different samples and that signal response in ICP-MS is dependent only on the ablated mass. Both assumptions ignore processes occurring in the ablation plume, so such mass normalization approaches have limited utility.

Sample preparation can introduce experimental artifacts and, therefore, has been extensively investigated and validated to ensure accurate quantification. Metal concentrations are affected by the extent to which metals are either added to or removed from the sample in the sample preparation and storage steps. Leaching of the metals during tissue embedding, freezing, and long-term storage has been reported. Snap freezing in liquid nitrogen reduces metal loss during sample preparation but does not completely eliminate it. Sample contamination during sectioning can be minimized by using metal-free blades and clean glass slides.

Although no common calibration method works for all types of biological samples, a majority of quantification approaches in LA-ICP-MS use matrix-matched standards, which effectively compensate for both fractionation and matrix effects. Matrix effects in ICP-MS are most pronounced for heavy elements with low ionization potentials, and such effects increase with increases in the concentration. Ideally, certified reference materials (CRMs) are used in these experiments. However, only a limited number of CRMs are available for biological tissue imaging experiments. As a result, substantial effort has been dedicated to the development of custom laboratory-prepared standards, including tissue homogenate spiked with standards containing appropriate elements. Several procedures have been developed to ensure good control of the water content and homogeneity of the standard samples necessary for accurate quantification. However, assessing the extent of the mismatch between the water content in the standard and sample is difficult, which may affect the results of quantification.

Thin polymer films and films of spiked agarose gel have been examined as alternatives to matrix-matched tissue standards. Such films could enable the implementation of isotope-dilution mass spectrometry techniques in LA-ICP-MS imaging experiments. Gelatin thin films spiked with metal standards have been used for imaging of cerium oxide nanoparticles in different tissues,

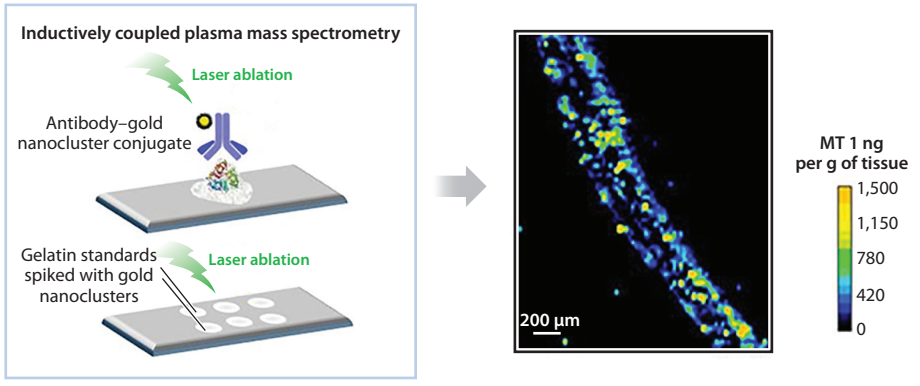


**Figure 7**

The innovative strategy shown here involves labeling tissue with antibodies conjugated with gold nanoclusters, which enables quantitative mass spectrometry imaging of the MT protein with high sensitivity and accuracy. Abbreviation: MT, metallothionein. Figure adapted with permission from Reference 88; copyright 2018 American Chemical Society.

providing insights into the origin of nanoparticle toxicity (86). Matrix-matched gelatin standards also have been used to support quantitative super-resolution imaging using LA-ICP-MS (87).

Another innovative strategy involving labeling with antibodies conjugated with gold nanoclusters (AuNCs) has been introduced to enable highly sensitive protein detection and accurate quantification (88). In this approach, an antibody was labeled with AuNCs using carbodiimide cross-linking, and the resulting bioconjugate was used for tissue staining, as illustrated in **Figure 7**. The stoichiometry of the bioconjugate was confirmed to be 1:1, and the size of an individual AuNC was 2.7 ± 0.1 nm, corresponding to an average of 579 Au atoms per bioconjugate. This labeling approach resulted in a substantial increase in the $Au^+$ signal in ICP-MS, which is referred to as signal amplification. Gelatin matrix-matched internal standards were prepared using established approaches and analyzed in parallel with the stained tissue sections. This approach was also used for the quantitative imaging of metallothioneins in human retinal tissue sections. Calibration curves were obtained for two different standards (AuNCs and $NaAuCl_4 \cdot H_2O$), which showed similar sensitivity, indicating that gelatin films spiked with $NaAuCl_4$ are appropriate standards for quantification. The observed localization of metallothioneins in retinal tissues was consistent with literature results, and the average concentrations were consistent with the results obtained for tissue homogenates using enzyme-linked immunosorbent assay (ELISA).

A similar approach was used to measure iron and ferroportin in the hippocampus of Alzheimer's disease patients (89). The same tissues were analyzed using fluorescence microscopy and LA-ICP-MS. Ferroportin expression was also evaluated using conventional immunohistochemistry. Because the uncertainty in the diameter of AuNCs contributes to the uncertainty in protein quantification, the researchers synthesized more homogeneous 2.20 ± 0.04–nm AuNCs containing an average of 314 Au atoms. In contrast with traditional methods, the immunohistochemistry-based LA-ICP-MS enables the imaging of both total and protein-bound iron. Other strategies for absolute protein quantification using ICP-MS have been summarized in a recent review (90).

## 5. CONCLUSIONS AND OUTLOOK

QMSI experiments present challenges and opportunities. Accurate quantification achieved using LA-ICP-MS techniques has been extensively validated. Meanwhile, QMSI using soft ionization

techniques is still in the early stages of development, and detailed assessment of the accuracy and reproducibility of the existing approaches must be performed. Matrix effects present a major challenge for quantifying ionization efficiency in QMSI experiments and must be accounted for to enable accurate quantification. Furthermore, the extraction efficiency of analytes must be further improved and quantified. Despite these challenges, QMSI based on soft ionization techniques has already provided important insights into the localization and abundance of small metabolites and lipids in tissue sections. Several innovative approaches have been developed to enable either the targeted or untargeted quantification of proteins in MSI experiments. Further improvements in the spatial resolution and throughput of nanoPOTS and related techniques will open new directions in untargeted, spatially resolved proteomics.

New approaches for QMSI are emerging to expand the range of compounds amenable to quantification and improve the accuracy of these experiments. For example, photocleavable probes have been used for the quantification of glycans, which are difficult to detect in MSI experiments due to their low ionization efficiency and signal suppression (91). The probes were designed to selectively target amino groups and contained chromophores that were cleaved using a 355-nm laser. Using four different probes, four types of glycans in single cells and tissues were observed. Matrix-free laser desorption ionization techniques show promise for broadening the molecular coverage in laser-based QMSI experiments (92, 93). Similarly, the parameter space of solvent dopants used in liquid-extraction-based QMSI techniques has not been fully explored.

New online derivatization approaches, along with optimization of the extraction solvent composition for a specific system, will enable the imaging of species with low ionization efficiency in tissue samples. The coupling of MSI with ion mobility separation has been used to both improve molecular coverage and facilitate the identification of biomolecules in tissue samples (94–96). The implementation of QMSI with ion mobility separation is a natural next step in the development of this promising technique. Finally, validated approaches that facilitate the simultaneous quantification of multiple classes of compounds will increase the experimental throughput.

## DISCLOSURE STATEMENT

The authors are not aware of any affiliations, memberships, funding, or financial holdings that might be perceived as affecting the objectivity of this review. Any opinions, findings, and conclusions or recommendations expressed in this material are those of the authors and do not necessarily reflect the views of the National Science Foundation or the National Institutes of Health.

## ACKNOWLEDGMENTS

The authors acknowledge support from the National Science Foundation (grant NSF-1808136) and the National Institutes of Health (NIH) Common Fund through the Office of Strategic Coordination and the Office of the NIH Director, Human Biomolecular Atlas Program (HuBMAP) (award UG3HL145593), both to J.L. D.M.S. acknowledges support from the National Science Foundation Graduate Research Fellowship (grant DGE-1333468).

## LITERATURE CITED

1. Fenn JB, Mann M, Meng CK, Wong SF, Whitehouse CM. 1990. Electrospray ionization–principles and practice. *Mass Spectrom. Rev.* 9(1):37–70
2. Hillenkamp F, Karas M, Beavis RC, Chait BT. 1991. Matrix-assisted laser desorption/ionization mass spectrometry of biopolymers. *Anal. Chem.* 63(24):1193A–203A
3. Norris JL, Caprioli RM. 2013. Analysis of tissue specimens by matrix-assisted laser desorption/ionization imaging mass spectrometry in biological and clinical research. *Chem. Rev.* 113(4):2309–42

4. Wu C, Dill AL, Eberlin LS, Cooks RG, Ifa DR. 2013. Mass spectrometry imaging under ambient conditions. *Mass Spectrom. Rev.* 32(3):218–43
5. Watrous JD, Dorrestein PC. 2011. Imaging mass spectrometry in microbiology. *Nat. Rev. Microbiol.* 9(9):683–94
6. Swales JG, Hamm G, Clench MR, Goodwin RJA. 2019. Mass spectrometry imaging and its application in pharmaceutical research and development: a concise review. *Int. J. Mass Spectrom.* 437:99–112
7. Buchberger AR, DeLaney K, Johnson J, Li L. 2018. Mass spectrometry imaging: a review of emerging advancements and future insights. *Anal. Chem.* 90(1):240–65
8. Rubakhin SS, Jurchen JC, Monroe EB, Sweedler JV. 2005. Imaging mass spectrometry: fundamentals and applications to drug discovery. *Drug Discov. Today* 10(12):823–37
9. McDonnell LA, Heeren RMA. 2007. Imaging mass spectrometry. *Mass Spectrom. Rev.* 26(4):606–43
10. Trufelli H, Palma P, Famiglini G, Cappiello A. 2011. An overview of matrix effects in liquid chromatography–mass spectrometry. *Mass Spectrom. Rev.* 30(3):491–509
11. Taylor PJ. 2005. Matrix effects: the Achilles heel of quantitative high-performance liquid chromatography–electrospray–tandem mass spectrometry. *Clin. Biochem.* 38(4):328–34
12. Nagana Gowda GA, Djukovic D. 2014. Overview of mass spectrometry-based metabolomics: opportunities and challenges. *Methods Mol. Biol.* 1198:3–12
13. Lei Z, Huhman DV, Sumner LW. 2011. Mass spectrometry strategies in metabolomics. *J. Biol. Chem.* 286(29):25435–42
14. Khoury S, Canlet C, Lacroix MZ, Berdeaux O, Jouhet J, Bertrand-Michel J. 2018. Quantification of lipids: model, reality, and compromise. *Biomolecules* 8(4):174
15. Koivusalo M, Haimi P, Heikinheimo L, Kostiainen R, Somerharju P. 2001. Quantitative determination of phospholipid compositions by ESI-MS: effects of acyl chain length, unsaturation, and lipid concentration on instrument response. *J. Lipid Res.* 42:663–72
16. Bantscheff M, Schirle M, Sweetman G, Rick J, Kuster B. 2007. Quantitative mass spectrometry in proteomics: a critical review. *Anal. Bioanal. Chem.* 389:1017–31
17. Ong SE, Mann M. 2005. Mass spectrometry-based proteomics turns quantitative. *Nat. Chem. Biol.* 1:252–62
18. Caprioli RM, Farmer TB, Gile J. 1997. Molecular imaging of biological samples: localization of peptides and proteins using MALDI-TOF MS. *Anal. Chem.* 69(23):4751–60
19. Cornett DS, Reyzer ML, Chaurand P, Caprioli RM. 2007. MALDI imaging mass spectrometry: molecular snapshots of biochemical systems. *Nat. Methods* 4:828–33
20. Walch A, Rauser S, Deininger SO, Höfler H. 2008. MALDI imaging mass spectrometry for direct tissue analysis: a new frontier for molecular histology. *Histochem. Cell Biol.* 130(3):421–34
21. Chen H, Gamez G, Zenobi R. 2009. What can we learn from ambient ionization techniques? *J. Am. Soc. Mass Spectrom.* 20(11):1947–63
22. Laskin J, Lanekoff I. 2016. Ambient mass spectrometry imaging using direct liquid extraction techniques. *Anal. Chem.* 88(1):52–73
23. Ifa DR, Wu C, Ouyang Z, Cooks RG. 2010. Desorption electrospray ionization and other ambient ionization methods: current progress and preview. *Analyst* 135(4):669–81
24. Venter AR, Douglass KA, Shelley JT, Hasman G, Honarvar E. 2014. Mechanisms of real-time, proximal sample processing during ambient ionization mass spectrometry. *Anal. Chem.* 86(1):233–49
25. Nemes P, Vertes A. 2007. Laser ablation electrospray ionization for atmospheric pressure, in vivo, and imaging mass spectrometry. *Anal. Chem.* 79(21):8098–106
26. Sampson JS, Hawkridge AM, Muddiman DC. 2006. Generation and detection of multiply-charged peptides and proteins by matrix-assisted laser desorption electrospray ionization (MALDESI) Fourier transform ion cyclotron resonance mass spectrometry. *J. Am. Soc. Mass Spectrom.* 17(12):1712–16
27. Takáts Z, Wiseman JM, Gologan B, Cooks RG. 2004. Mass spectrometry sampling under ambient conditions with desorption electrospray ionization. *Science* 306(5695):471–73
28. Wiseman JM, Ifa DR, Zhu Y, Kissinger CB, Manicke NE, et al. 2008. Desorption electrospray ionization mass spectrometry: imaging drugs and metabolites in tissues. *PNAS* 105(47):18120–25
29. Roach PJ, Laskin J, Laskin A. 2010. Nanospray desorption electrospray ionization: an ambient method for liquid-extraction surface sampling in mass spectrometry. *Analyst* 135:2233–36

30. Van Berkel GJ, Sanchez AD, Quirke JME. 2002. Thin-layer chromatography and electrospray mass spectrometry coupled using a surface sampling probe. *Anal. Chem.* 74(24):6216–23
31. Kertesz V, Van Berkel GJ. 2010. Fully automated liquid extraction-based surface sampling and ionization using a chip-based robotic nanoelectrospray platform. *J. Mass Spectrom.* 45(3):252–60
32. Lietz CB, Gemperline E, Li L. 2013. Qualitative and quantitative mass spectrometry imaging of drugs and metabolites. *Adv. Drug Deliv. Rev.* 65(8):1074–85
33. Lanekoff I, Laskin J. 2018. Quantitative mass spectrometry imaging of molecules in biological systems. In *Advances in Chromatography*, Vol. 54, ed. E Grushka, N Grinberg, pp. 43–72. Boca Raton, FL: CRC Press
34. Porta T, Lesur A, Varesio E, Hopfgartner G. 2015. Quantification in MALDI-MS imaging: What can we learn from MALDI-selected reaction monitoring and what can we expect for imaging? *Anal. Bioanal. Chem.* 407(8):2177–87
35. Ellis SR, Bruinen AL, Heeren RMA. 2014. A critical evaluation of the current state-of-the-art in quantitative imaging mass spectrometry. *Anal. Bioanal. Chem.* 406(5):1275–89
36. Lanekoff I, Stevens SL, Stenzel-Poore MP, Laskin J. 2014. Matrix effects in biological mass spectrometry imaging: identification and compensation. *Analyst* 139(14):3528–32
37. Rohner TC, Staab D, Stoeckli M. 2005. MALDI mass spectrometric imaging of biological tissue sections. *Mech. Ageing Dev.* 126(1):177–85
38. Lanekoff I, Thomas M, Carson JP, Smith JN, Timchalk C, Laskin J. 2013. Imaging nicotine in rat brain tissue by use of nanospray desorption electrospray ionization mass spectrometry. *Anal. Chem.* 85(2):882–89
39. Bergman HM, Lundin E, Andersson M, Lanekoff I. 2016. Quantitative mass spectrometry imaging of small-molecule neurotransmitters in rat brain tissue sections using nanospray desorption electrospray ionization. *Analyst* 141(12):3686–95
40. Taylor AJ, Dexter A, Bunch J. 2018. Exploring ion suppression in mass spectrometry imaging of a heterogeneous tissue. *Anal. Chem.* 90(9):5637–45
41. Perry WJ, Patterson NH, Prentice BM, Neumann EK, Caprioli RM, Spraggins JM. 2019. Uncovering matrix effects on lipid analyses in MALDI imaging mass spectrometry experiments. *J. Mass Spectrom.* 55(4):e4491
42. Yang C, Lee HK, Zhang Y, Jiang LL, Chen ZF, et al. 2019. In situ detection and imaging of PFOS in mouse kidney by matrix-assisted laser desorption/ionization imaging mass spectrometry. *Anal. Chem.* 91(14):8783–88
43. Rzagalinski I, Kovačević B, Hainz N, Meier C, Tschernig T, Volmer DA. 2018. Toward higher sensitivity in quantitative MALDI imaging mass spectrometry of CNS drugs using a nonpolar matrix. *Anal. Chem.* 90(21):12592–600
44. Sugiyama E, Masaki N, Matsushita S, Setou M. 2015. Ammonium sulfate improves detection of hydrophilic quaternary ammonium compounds through decreased ion suppression in matrix-assisted laser desorption/ionization imaging mass spectrometry. *Anal. Chem.* 87(22):11176–81
45. Barré FPY, Flinders B, Garcia JP, Jansen I, Huizing LRS, et al. 2016. Derivatization strategies for the detection of triamcinolone acetonide in cartilage by using matrix-assisted laser desorption/ionization mass spectrometry imaging. *Anal. Chem.* 88(24):12051–59
46. Unsihuay D, Qiu J, Swaroop S, Nagornov KO, Kozhinov AN, et al. 2020. Imaging of triglycerides in tissues using nanospray desorption electrospray ionization (nano-DESI) mass spectrometry. *Int. J. Mass Spectrom.* 448:116269
47. Eberlin LS, Ferreira CR, Dill AL, Ifa DR, Cheng L, Cooks RG. 2011. Nondestructive, histologically compatible tissue imaging by desorption electrospray ionization mass spectrometry. *ChemBioChem* 12(14):2129–32
48. Duncan KD, Fang R, Yuan J, Chu RK, Dey SK, et al. 2018. Quantitative mass spectrometry imaging of prostaglandins as silver ion adducts with nanospray desorption electrospray ionization. *Anal. Chem.* 90(12):7246–52
49. Lostun D, Perez CJ, Licence P, Barrett DA, Ifa DR. 2015. Reactive DESI-MS imaging of biological tissues with dicationic ion-pairing compounds. *Anal. Chem.* 87(6):3286–93
50. Wu C, Ifa DR, Manicke NE, Cooks RG. 2009. Rapid, direct analysis of cholesterol by charge labeling in reactive desorption electrospray ionization. *Anal. Chem.* 81(18):7618–24

51. Rzagalinski I, Volmer DA. 2017. Quantification of low molecular weight compounds by MALDI imaging mass spectrometry–a tutorial review. *Biochim. Biophys. Acta Proteins Proteom.* 1865(7):726–39
52. Chumbley CW, Reyzer ML, Allen JL, Marriner GA, Via LE, et al. 2016. Absolute quantitative MALDI imaging mass spectrometry: a case of rifampicin in liver tissues. *Anal. Chem.* 88(4):2392–98
53. Hansen HT, Janfelt C. 2016. Aspects of quantitation in mass spectrometry imaging investigated on cryosections of spiked tissue homogenates. *Anal. Chem.* 88(23):11513–20
54. Barry JA, Groseclose MR, Castellino S. 2019. Quantification and assessment of detection capability in imaging mass spectrometry using a revised mimetic tissue model. *Bioanalysis* 11(11):1099–116
55. Song X, He J, Li C, Sun C, Pang X, et al. 2019. Fabrication of homogenous three-dimensional biomimetic tissue for mass spectrometry imaging. *J. Mass Spectrom.* 54(5):378–88
56. Giordano S, Morosi L, Veglianese P, Licandro SA, Frapolli R, et al. 2016. 3D mass spectrometry imaging reveals a very heterogeneous drug distribution in tumors. *Sci. Rep.* 6:37027
57. Nazari M, Bokhart MT, Loziuk PL, Muddiman DC. 2018. Quantitative mass spectrometry imaging of glutathione in healthy and cancerous hen ovarian tissue sections by infrared matrix-assisted laser desorption electrospray ionization (IR-MALDESI). *Analyst* 143:654–61
58. Grey AC, Demarais NJ, West BJ, Donaldson PJ. 2019. A quantitative map of glutathione in the aging human lens. *Int. J. Mass Spectrom.* 437:58–68
59. Barry JA, Ait-Belkacem R, Hardesty WM, Benakli L, Andonian C, et al. 2019. Multicenter validation study of quantitative imaging mass spectrometry. *Anal. Chem.* 91(9):6266–74
60. Prentice BM, Chumbley CW, Hachey BC, Norris JL, Caprioli RM. 2016. Multiple time-of-flight/time-of-flight events in a single laser shot for improved matrix-assisted laser desorption/ionization tandem mass spectrometry quantification. *Anal. Chem.* 88(19):9780–88
61. Prentice BM, Chumbley CW, Caprioli RM. 2017. Absolute quantification of rifampicin by MALDI imaging mass spectrometry using multiple TOF/TOF events in a single laser shot. *J. Am. Soc. Mass Spectrom.* 28(1):136–44
62. Deepaisarn S, Tar PD, Thacker NA, Seepujak A, McMahon AW. 2018. Quantifying biological samples using linear Poisson independent component analysis for MALDI-ToF mass spectra. *Bioinformatics* 34(6):1001–8
63. Kertesz V, Weiskittel TM, Vavrek M, Freddo C, Van Berkel GJ. 2016. Extraction efficiency and implications for absolute quantitation of propranolol in mouse brain, liver and kidney tissue sections using droplet-based liquid microjunction surface sampling high-performance liquid chromatography/electrospray ionization tandem mass spectrometry. *Rapid Commun. Mass Spectrom.* 30(14):1705–12
64. Lanekoff I, Thomas M, Laskin J. 2014. Shotgun approach for quantitative imaging of phospholipids using nanospray desorption electrospray ionization mass spectrometry. *Anal. Chem.* 86(3):1872–80
65. Chen X, Hatsis P, Judge J, Argikar UA, Ren X, et al. 2016. Compound property optimization in drug discovery using quantitative surface sampling micro liquid chromatography with tandem mass spectrometry. *Anal. Chem.* 88(23):11813–20
66. Cahill JF, Kertesz V, Weiskittel TM, Vavrek M, Freddo C, Van Berkel GJ. 2016. Online, absolute quantitation of propranolol from spatially distinct 20- and 40-μm dissections of brain, liver, and kidney thin tissue sections by laser microdissection–liquid vortex capture–mass spectrometry. *Anal. Chem.* 88(11):6026–34
67. Wu Q, Huang Z, Wang Y, Zhang Z, Lu H. 2020. Absolute quantitative imaging of sphingolipids in brain tissue by exhaustive liquid microjunction surface sampling–liquid chromatography–mass spectrometry. *J. Chromatogr. A* 1609:460436
68. Swales JG, Strittmatter N, Tucker JW, Clench MR, Webborn PJH, Goodwin RJA. 2016. Spatial quantitation of drugs in tissues using liquid extraction surface analysis mass spectrometry imaging. *Sci. Rep.* 6:37648
69. Luo Z, He J, He J, Huang L, Song X, et al. 2018. Quantitative analysis of drug distribution by ambient mass spectrometry imaging method with signal extinction normalization strategy and inkjet-printing technology. *Talanta* 179:230–37
70. Shariatgorji M, Strittmatter N, Nilsson A, Källback P, Alvarsson A, et al. 2016. Simultaneous imaging of multiple neurotransmitters and neuroactive substances in the brain by desorption electrospray ionization mass spectrometry. *NeuroImage* 136:129–38

71. Song X, He J, Pang X, Zhang J, Sun C, et al. 2019. Virtual calibration quantitative mass spectrometry imaging for accurately mapping analytes across heterogenous biotissue. *Anal. Chem.* 91(4):2838–46
72. Stoeckli M, Chaurand P, Hallahan DE, Caprioli RM. 2001. Imaging mass spectrometry: a new technology for the analysis of protein expression in mammalian tissues. *Nat. Med.* 7:493–96
73. Groseclose MR, Andersson M, Hardesty WM, Caprioli RM. 2007. Identification of proteins directly from tissue: *in situ* tryptic digestions coupled with imaging mass spectrometry. *J. Mass Spectrom.* 42(2):254–62
74. Crecelius A, Caprioli R, Williams B, Dawant B, Bodenheimer B. 2005. Three-dimensional visualization of protein expression in mouse brain structures using imaging mass spectrometry. *J. Am. Soc. Mass Spectrom.* 16(7):1093–99
75. Havlikova J, Randall EC, Griffiths RL, Swales JG, Goodwin RJA, et al. 2019. Quantitative imaging of proteins in tissue by stable isotope labeled mimetic liquid extraction surface analysis mass spectrometry. *Anal. Chem.* 91(22):14198–202
76. Zhu Y, Dou M, Piehowski PD, Liang Y, Wang F, et al. 2018. Spatially resolved proteome mapping of laser capture microdissected tissue with automated sample transfer to nanodroplets. *Mol. Cell. Proteom.* 17(9):1864–74
77. Piehowski PD, Zhu Y, Bramer LM, Stratton KG, Zhao R, et al. 2020. Automated mass spectrometry imaging of over 2000 proteins from tissue sections at 100-μm spatial resolution. *Nat. Commun.* 11:8
78. Beauchemin D. 2008. Inductively coupled plasma mass spectrometry. *Anal. Chem.* 80(12):4455–86
79. Hare D, Austin C, Doble P. 2012. Quantification strategies for elemental imaging of biological samples using laser ablation-inductively coupled plasma-mass spectrometry. *Analyst* 137(7):1527–37
80. Durrant SF, Ward NI. 1994. Laser ablation-inductively coupled plasma-mass spectrometry (LA-ICP-MS) for the multielemental analysis of biological materials: a feasibility study. *Food Chem.* 49(3):317–23
81. Gray AL. 1985. Solid sample introduction by laser ablation for inductively coupled plasma source mass spectrometry. *Analyst* 110(5):551–56
82. Sussulini A, Becker JS, Becker JS. 2017. Laser ablation ICP-MS: application in biomedical research. *Mass Spectrom. Rev.* 36(1):47–57
83. Pozebon D, Scheffler GL, Dressler VL, Nunes MAG. 2014. Review of the applications of laser ablation inductively coupled plasma mass spectrometry (LA-ICP-MS) to the analysis of biological samples. *J. Anal. At. Spectrom.* 29(12):2204–28
84. Giesen C, Mairinger T, Khoury L, Waentig L, Jakubowski N, Panne U. 2011. Multiplexed immunohistochemical detection of tumor markers in breast cancer tissue using laser ablation inductively coupled plasma mass spectrometry. *Anal. Chem.* 83(21):8177–83
85. Todoli JL, Mermet JM. 1998. Study of polymer ablation products obtained by ultraviolet laser ablation—inductively coupled plasma atomic emission spectrometry. *Spectrochim. Acta B At. Spectrosc.* 53(12):1645–56
86. Chen B, Lum JT-S, Huang Y, Hu B, Leung KS-Y. 2019. Integration of sub-organ quantitative imaging LA-ICP-MS and fractionation reveals differences in translocation and transformation of $CeO_2$ and $Ce^{3+}$ in mice. *Anal. Chim. Acta* 1082:18–29
87. Westerhausen MT, Bishop DP, Dowd A, Wanagat J, Cole N, Doble PA. 2019. Super-resolution reconstruction for two- and three-dimensional LA-ICP-MS bioimaging. *Anal. Chem.* 91(23):14879–86
88. Cruz-Alonso M, Fernandez B, García M, González-Iglesias H, Pereiro R. 2018. Quantitative imaging of specific proteins in the human retina by laser ablation ICPMS using bioconjugated metal nanoclusters as labels. *Anal. Chem.* 90(20):12145–51
89. Cruz-Alonso M, Fernandez B, Navarro A, Junceda S, Astudillo A, Pereiro R. 2019. Laser ablation ICP-MS for simultaneous quantitative imaging of iron and ferroportin in hippocampus of human brain tissues with Alzheimer's disease. *Talanta* 197:413–21
90. Cid-Barrio L, Calderón-Celis F, Abásolo-Linares P, Fernández-Sánchez ML, Costa-Fernández JM, et al. 2018. Advances in absolute protein quantification and quantitative protein mapping using ICP-MS. *Trends Anal. Chem.* 104:148–59
91. Han J, Huang X, Liu H, Wang J, Xiong C, Nie Z. 2019. Laser cleavable probes for *in situ* multiplexed glycan detection by single cell mass spectrometry. *Chem. Sci.* 10(47):10958–62. Corrigendum. 2020. *Chem. Sci.* 11:1176

92. Muthu M, Gopal J, Chun S. 2017. Nanopost array laser desorption ionization mass spectrometry (NAPA-LDI MS): gathering moss? *Trends Anal. Chem.* 97:96–103
93. Korte AR, Morris NJ, Vertes A. 2019. High throughput complementary analysis and quantitation of metabolites by MALDI- and silicon nanopost array-laser desorption/ionization-mass spectrometry. *Anal. Chem.* 91(6):3951–58
94. Sans M, Feider CL, Eberlin LS. 2018. Advances in mass spectrometry imaging coupled to ion mobility spectrometry for enhanced imaging of biological tissues. *Curr. Opin. Chem. Biol.* 42:138–46
95. Woods AS, Jackson SN. 2010. The application and potential of ion mobility mass spectrometry in imaging MS with a focus on lipids. *Methods Mol. Biol.* 656:99–111
96. Kiss A, Heeren RMA. 2011. Size, weight and position: ion mobility spectrometry and imaging MS combined. *Anal. Bioanal. Chem.* 399:2623–34